REPORT

www.the-innovation.org

A new thiol-sulfur click chemistry for lithium-organosulfide batteries

Rong Zou,[1] Wenwu Liu,[1] and Fen Ran[1,*]

*Correspondence: ranfen@lut.edu.cn

Received: April 22, 2024; Accepted: December 10, 2024; Published: January 13, 2025; https://doi.org/10.1016/j.xinn.2024.100765

GRAPHICAL ABSTRACT

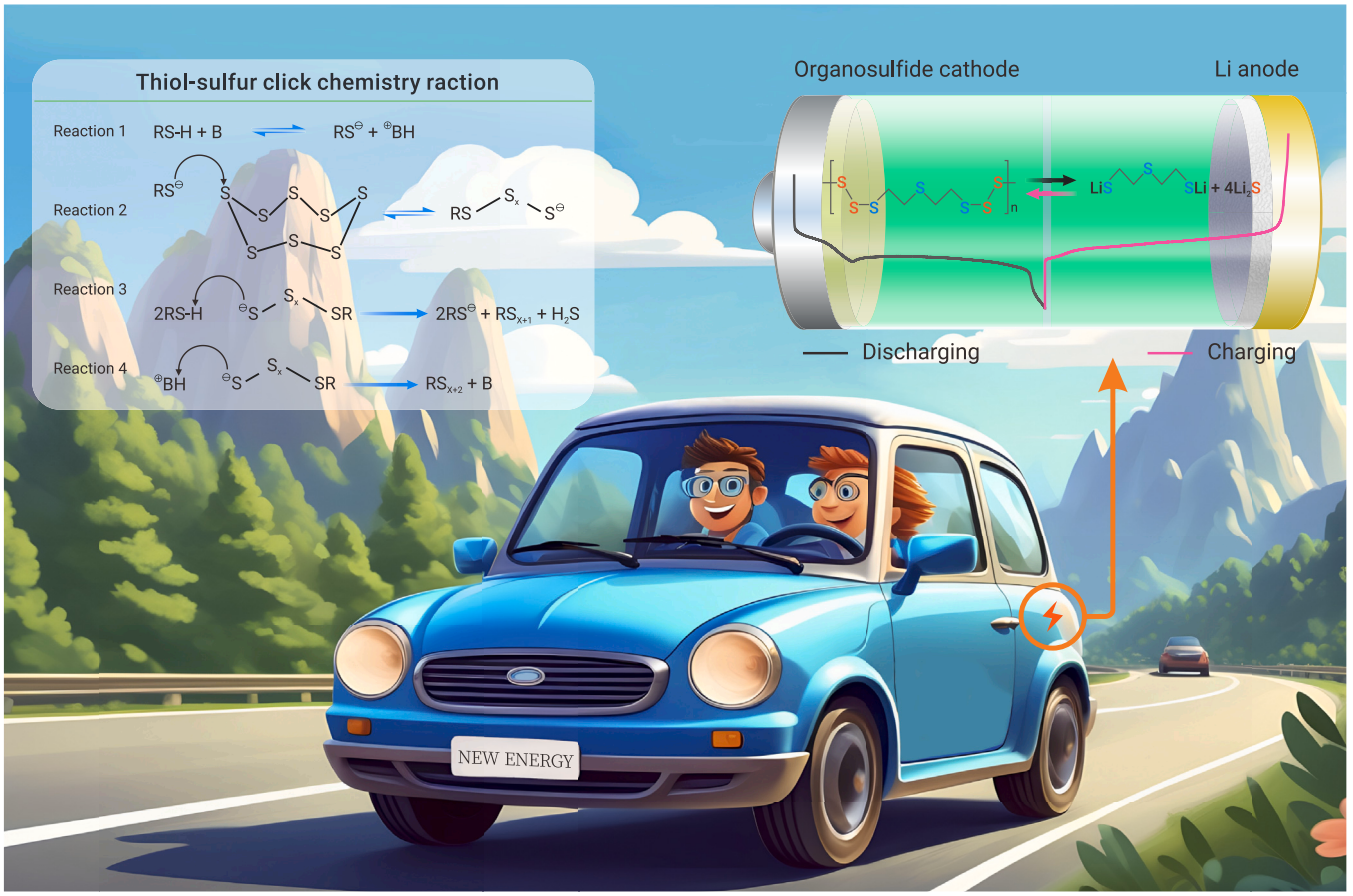

PUBLIC SUMMARY

- A new alkali-catalyzed thiol and sulfur reaction synthesis method, termed "thiol-sulfur click chemistry."
- Polydivinylthioether hexasulfide (PDVTHS), a novel sulfur-containing polymer, is designed and synthesized.
- PDVTHS exhibits excellent specific capacity for lithium-organosulfide batteries.
- PDVTHS significantly enhances the cyclability of lithium-organosulfide batteries.

OPEN ACCESS

REPORT

The Innovation

A new thiol-sulfur click chemistry for lithium-organosulfide batteries

Rong Zou,[1] Wenwu Liu,[1] and Fen Ran[1,*]

[1]State Key Laboratory of Advanced Processing and Recycling of Non-ferrous Metals, Department of Polymeric Materials Engineering, School of Materials Science and Engineering, Lanzhou University of Technology, Lanzhou 730050, China

*Correspondence: ranfen@lut.edu.cn

Received: April 22, 2024; Accepted: December 10, 2024; Published: January 13, 2025; https://doi.org/10.1016/j.xinn.2024.100765

Citation: Zou R., Liu W., and Ran F. (2025). A new thiol-sulfur click chemistry for lithium-organosulfide batteries. The Innovation **6(2)**, 100765.

Click chemistry is a rapid, reliable, and powerful function and a highly selective organic reaction that facilitates the efficient synthesis of various molecules by joining small units. This approach has found widespread applications in fields such as drug development, chemical synthesis, and molecular biology. In recent years, the reaction of alkali-catalyzed polymerization of thiol and sulfur has been employed to prepare various sulfur-containing polymers, which are applied as electrochemical active electrode materials in the pursuit of good performance. In this study, it is surprising to find that the reaction mechanism exhibits characteristics of both the alkali-catalyzed sulfhydryl Micheal addition reaction and thiol-epoxy click chemistry; for the first time, thiol-sulfur click chemistry is defined in detail, providing a comprehensive description of its underlying scientific principles. The introduction of this new reaction pathway holds significant potential for advancing research and the development of sulfur-containing polymers. Based on this novel click chemistry, a new sulfur-containing polymer, polydivinylthioether hexasulfide, has been designed and successfully applied as a cathode material in lithium-organosulfide batteries. This material demonstrates excellent electrochemical performance, achieving an initial capacity that reaches 790.5 mAh g^{-1} (82.6% of theoretical capacity), and in a long-term cycle test, the capacity decay rate is only 0.063% after 1,000 cycles.

INTRODUCTION

To solve the inherent defects of typic lithium-sulfur (Li-S) batteries, there has been growing interest in exploring alternative cathode materials that can better tolerate volume changes and mitigate the shuttle effect. In the 1980s, Visco and De Jonghe first proposed the use of the sulfur-containing polymer (SCP) tetraethylthiuram disulfide (TETD) as a cathode active material in secondary batteries. However, this idea did not gain significant attention at the time due to the low capacity. Nonetheless, it opened the door for further exploration of polymers as alternative cathode materials. Since then, various polymers have been studied as potential cathode materials of Li-S batteries, including benzoquinone, anthraquinone,[1,2] poly(pentacenetetrone sulfide),[3] phenyl tetrasulfide (PTS),[4] poly(vinylphenoxazine),[5] phenothiazine-based copolymers,[6] etc. Among these, SCPs have delivered decent properties that have attracted wide attention. Notably, Fu et al.[7] designed many innovative SCPs and successfully applied them in lithium-organosulfide batteries.

In previous works, we investigated sulfurized polyaniline (SPANI)[8,9] and sulfurized polyacrylonitrile (SPAN),[10] which demonstrated impressive performance in lithium-organosulfide batteries. Herein, a novel SCP, polydivinylthioether hexasulfide (*PDVTHS*) has been reported, synthesized by adopting 2, 2′-thiodiethanethiol (TDET) monomer and sulfur powder under base catalysis. Notably, the figures of merit of this reaction between thiol and sulfur (S_8) are its rapid reaction rate, mild reaction conditions occurring at room temperature, specific selectivity, and single product. These features align closely with the principles of click chemistry, a concept introduced by Sharpless in 2001.[11] Click chemistry refers to a class of fast, reliable, and highly selective organic reactions, primarily involving the assembly of small units to efficiently synthesize various molecules. Thiol click chemistry is the most important and widely used click chemistry, which encompasses two main reaction mechanisms: (1) the radical mechanism reaction. The year 2007, radical introduced thiol-ene reaction was firstly defined as click chemistry belonged to a free stepwise polymerization process. (2) The nucleophilic mechanism reaction, which includes the thiol-isocyanate reaction, thiol-epoxy reaction, and thiol-ene reaction, where the nucleophilic nature of the thiol or sulfur anion enables it to attack the reactive functional group.

Based on an analysis of the reaction mechanism of thiol and sulfur (S_8) under base catalysis, this work proposes an innovative type of click chemistry reaction, referred to as thiol-sulfur click chemistry. This reaction exhibits characteristics similar to both the thiol-Micheal addition reaction[12–14] and thiol-epoxy click chemistry.[11,15,16] The proposal of the new reaction mechanism offers significant insights for the research and development of other SCPs. In addition, a new SCP, *PDVTHS*, was synthesized using this thiol-sulfur click chemistry and successfully used in lithium-organosulfide batteries. Specifically, the rate capacity at different current densities ranging from 0.05 to 0.5 C can reach 790.5 (82.6% of theoretical capacity), 671, 649, and 609 mAh g^{-1}, respectively. In terms of long-term cycling performance at 0.2 C (*PDVTHS* loading of 2.48 mg cm^{-2}), the initial capacity is 335 mAh g^{-1}, which remains at 124 mAh g^{-1} after 1,000 cycles, corresponding to a capacity decay rate of only 0.063%.

MATERIALS AND METHODS

Materials and chemicals

Sulfur (S_8, ≥99.5%, *Canrd*), TDET ($C_4H_{10}S_3$, >97% GC, *Macklin*), buckypaper (*Nanotechlab*), and Li-S battery electrolyte (1.0 M LiTFSI in DOL:DME = 1:1 vol % with 2.0% $LiNO_3$, *Canrd*) were purchased and used as received. Celgard 2500 was used as the separator (*Canrd*). Other chemicals, including methylbenzene (PhMe), carbon disulfide (CS_2), and diethylamine (Et_2NH) were purchased from Chemical Reagents, China, and used as received at analytical grade.

Synthesis of *PDVTHS*

The synthesis procedure took place inside an argon-filed glovebox (<1 ppm of H_2O and O_2, Mikrouna). S_8 and TDET were added to a MePh/CS_2 (v:v = 1:1) mixture with the equiv ratio of 5:1, followed by vigorous stirring until all the reactant dissolved and then the addition of 5 μL of diethylamine (Et_2NH) as a catalyst. Subsequently, H_2S gas was observed effervescently and subsided after about 10–15 min. The resulting solution was immediately injected onto the buckypaper to form the cathode. The remaining solution was stirred overnight, resulting in the precipitation of the SCP PDVTHS. Finally, the target product, *PDVTHS*, was transfer to a 60° oven for drying prior to further detection and characterization.

Synthesis of *PDVTHS*-CNT cathode

Buckypaper was punched into discs with 12 mm diameters and dried for 12 h in a vacuum oven; then, 20 μL of the *PDVTHS* solution was injected onto a tailored CNT paper disc (typically 0.01 mmol or 2.8 mg active material). *PDVTHS*-CNT was allowed to complete the reaction *in situ*, accompanied by a slow precipitation of the *PDVTHS* polymer when CS_2 evaporated. Thus, the achieved *PDVTHS*-CNT cathode had an SCP area loading of 2.47 mg cm^{-2}. This synthesized procedure was conducted within an argon-filed glovebox.

Materials characterization

The microstructures for the *PDVTHS*-CNT cathode were observed by a field-emission scanning electron microscope (FE-SEM; JEOL, JSM-6701F, Japan). The element distribution was analyzed by EDS mapping (Zeiss Gemini300). The detailed element contents of S, C, and H were detected on an element analyzer (EA). XRD patterns were recorded using an X-ray powder diffraction map (XRD, D8 ADVANCE, Bruker) with Cu Kα radiation (λ = 0.1541 nm). Fourier transform infrared spectroscopy (FTIR spectroscopy; Bruker, Vectory-80, Germany) spectra were recorded from 4,000 to 400 cm^{-1}. The pristine *PDVTHS* polymer are characterized by the Raman spectrum (Raman, HORIBA, XploRA Plus, China) with a wavelength range of 100–2,000 cm^{-1}. The molecular weight and molecular simplification of the target compounds were characterized by a time-of-flight secondary ion mass spectrometer (TOF-SIMS; IONTOF 5). X-ray photoelectron spectroscopy (XPS; ESCALAB 250Xi, Thermo Fisher Scientific) patterns were calibrated using the C 1*s* peak at 284.8 eV to analyze the bonding energy value of the *PDVTHS* polymer and the *PDVTHS*-CNT cathode of completely discharge under 0.05 C of current density after 2 cycles. Thermogravimetric analysis (TGA; Discovery TGA, USA) and differential scanning calorimetry (DSC; Neschi STA449C synchronous thermal analysis equipment) of the *PDVTHS* polymer were performed from 25°C to 800°C with a heating rate of 10°C min^{-1} in an argon atmosphere.

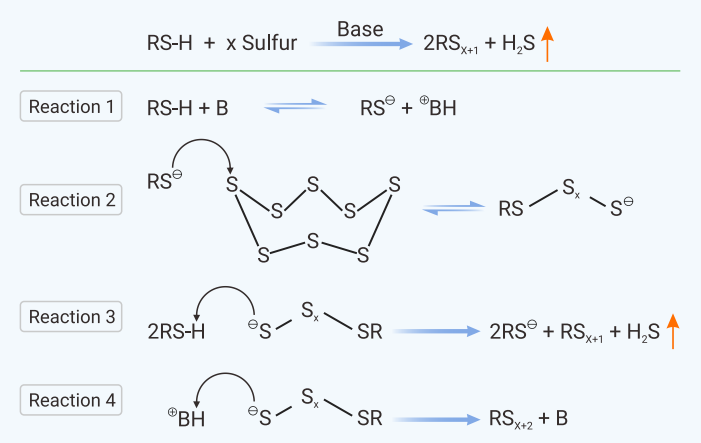

Figure 1. Thiol-sulfur click chemistry reaction under alkali-catalyzed B, base.

UV-visible (UV-vis) absorption spectra (Shimadzu UV-3600) were used to measure discharging/recharging mediate products.

Electrochemical measurements

CR2032-type coin cells were fabricated in an argon-filled glovebox. The *PDVTHS*-CNT cathode was assembled with a lithium anode, and Celgard 2500 was placed between the cathode and anode as a separator. Then, 20 μL of the commercial Li-S electrolyte was added on either side of the separator. Cells were crimped and tested by cyclic voltammetry (CV) through an electrochemical workstation (CHI760E, Shanghai, China) between 1.6 and 3 V with a sweep speed of 50 μV s^{-1}. Electrochemical impedance spectroscopy (EIS) was also performed on an electrochemical workstation (CHI760E) to explore the charge transfer resistant (R_{ct}) change before and after cycling with frequency ranges from 100 kHz to 0.01 Hz. A land battery cycler (CT2001A, Wuhan, China) measured the capacity properties at different C rates (1 C = 957.3 mA g^{-1}), galvanostatic charging discharging (GCD) profiles, and cycling lifetimes within a voltage window of 1.6–3 V.

Operando Raman spectroscopy analysis

A Li-S battery consistent with the button battery was assembled with an *in situ* Raman device (HORIBA, Horiba LabRAM HR Evolution, France) with laser excitation at 633 nm. The battery was continuously tested under CV patterns with a sweep speed of 50 μV s^{-1} during the whole Raman spectrum collection process. The Raman spectrum simultaneously recorded different discharging/recharging voltage depths.

RESULTS AND DISCUSSION

The thiol-sulfur reaction catalyzed by alkali (Figure 1) shares characteristics with both the thiol-epoxy reaction and the alkali-catalyzed Michael addition reaction. A stepwise depiction is used to simplify the process for better understanding. Due to the influence of the lone pair of electrons on the S atom, an asymmetric sp^3 structure with a triangular cone structure is formed. S_8 rendered a corn-shaped ring structure that appeared at a certain ring tension, which is vulnerable to nucleophile attack. Although thiol groups can be involved in such ring-opening reactions, the thiol-sulfur reaction cannot be carried out, even when the thiol group collides with a ring-tensioned molecule, due to the weak nucleophilicity of the thiol group. Thiol functional groups exhibit a strong nucleophilic ability only when they form sulfur anions under the action of alkaline catalysts. These anions can nucleophilically attack the less resistant S atom on the upper part of the S_8 ring. The resulting sulfur anion intermediates not only capture H protons from thiol groups or conjugated acids because of their strong alkalinity but also nucleophilically attack conjugated acids formed by alkali catalysts. The two anion multiplication steps (reactions 1 and 2) in this reaction closely resemble the "insertion-capture" multiplication process in the thiol-ene radical addition.[12] After initiation, the reaction proceeds rapidly without interference from other proton sources, such as water or alcohol.

The thiol-sulfur reaction belongs to the thiol click chemistry of the nucleophilic mechanism, and its reaction mechanism proceeds as follows. (1) Under the influence of an alkaline catalyst, the thiol group loses a hydrogen proton, forming the sulfur anion and conjugate acid of the catalyst (reaction 1). (2) The sulfur anion, a strong nucleophile, attacks the less resistant sulfur atom at the upper part of the S_8 ring. The alkoxide anion with strong alkalinity intermediates is formed by S_8 after ring opening (reaction 2). (3) The alkoxide anions snatch the protons from the thiol group, forming sulfur anions and sulfane, leading to a large amount of hydrogen (reaction 3). The resulting sulfur anions continue to nucleophilically attack unreacted S_8 molecules (reaction 2). (4) Finally, alkoxide anions snatch the protons from the conjugated acid of the catalyst (reaction 4), regenerating the base catalyst.

The rate-limiting step in thiol-sulfur click chemistry is the nucleophilic attack process on the eight-membered ring of S_8 by the sulfur anion. The reaction rate is expressed as Equation 1:

$$R_{rxn} = k[R - S^-][\text{sulfur}] \quad \text{(Equation 1)}$$

$[R - S^-]$ is the concentration of the sulfur anion that is obtained by the equilibrium formula of mercaptan and base.

$$K_{eq} = \frac{[R - S^-][B^+ - H]}{[R - SH][B]} \quad \text{(Equation 2)}$$

Therefore,

$$R_{rxn} = kK_{eq}\left(\frac{[B]}{[B^+ - H]}\right)[R - SH][\text{sulfur}] \quad \text{(Equation 3)}$$

The rate of the thiol-sulfur click chemistry reaction is related to the following three points from Equation 3: the concentration of the solvent, the alkalinity of the catalyst, and the acidity of the mercaptan (which is related to the structure of the mercaptan).

The acidity of mercaptans varies due to differences in their structures, and this variation influences the reaction rate. The specific relationship between structure and acidity can be seen in Figure S1. In general, thiol groups are categorized into four types: thiopropionate, aromatic mercaptan, mercaptoacetate, and aliphatic mercaptan. Their pKa values follow this order: thiopropionate < aromatic mercaptan < thioglycolate < aliphatic mercaptan. According to the principle that a higher pKa value corresponds to a weaker acid, the acidity of mercaptans is ranked as thiopropionate > aromatic mercaptan > thioglycolate > aliphatic mercaptan. In the case of weak base catalysis, the concentration of sulfur ions depends on the balance between mercaptan and the base catalyst.

In previous reports, the preparation of SCPs has typically involved the use of rhombic S_8 crystals and organic precursors through vulcanization and inverse vulcanization, processes that require high-temperature annealing. The rhombic structure of S_8 crystals is destructed until temperatures greater than 95°C, and the ring-opening polymerization of S_8 is triggered at temperatures above 159°C.[17] To obtain an SCP with a well-defined chemical structure and controlled sulfur chain length, the temperature of the synthesis must be below 95°C. In this work, the proposed base-catalyzed thiol-sulfur reaction offers several advantages, including mild reaction conditions, room temperature reactivity, rapid processing, and high selectivity. The high acidity of the thiol group enhances its ability to participate in thiol-sulfur click chemistry through a nucleophilic mechanism. Additionally, the corn-shaped ring structure of S_8 promotes nucleophilic ring-opening reactions.

PDVTHS is prepared by a thiol-sulfur click reaction involving TDET and sulfur powder. Figure 2A illustrates the reaction equation for the synthesis of *PDVTHS*. 1 equiv TDET and 5 equiv sulfur powder are dissolved in a 4 mL mixture of toluene ($C_6H_5CH_3$, PhMe) and carbon disulfide (CS_2) (v:v = 1:1), resulting in a clear yellow solution. Upon the addition of an ethylenediamine catalyst ($(Et)_2NH$), a significant amount of H_2S gas is released. Gas evolution subsided after about 10 min, and the resulting solution was still clear and transparent. The solution is then immediately added to the CNT paper. Figure S2 describes the mechanism according to the thiol-sulfur click reaction. TDET being catalyzed by the alkaline catalyst to form a sulfur anion, a strong nucleophile, is a vital process. Furthermore, the sulfur anion attacks the S_8 ring by ring-opening polymerization to produce *PDVTHS*.

The *PDVTHS*-CNT cathode and residual polymer solution are placed in an argon-filled glovebox to dry overnight, allowing the completion of the reaction *in situ* accompanied by slow precipitation of the *PDVTHS* polymer

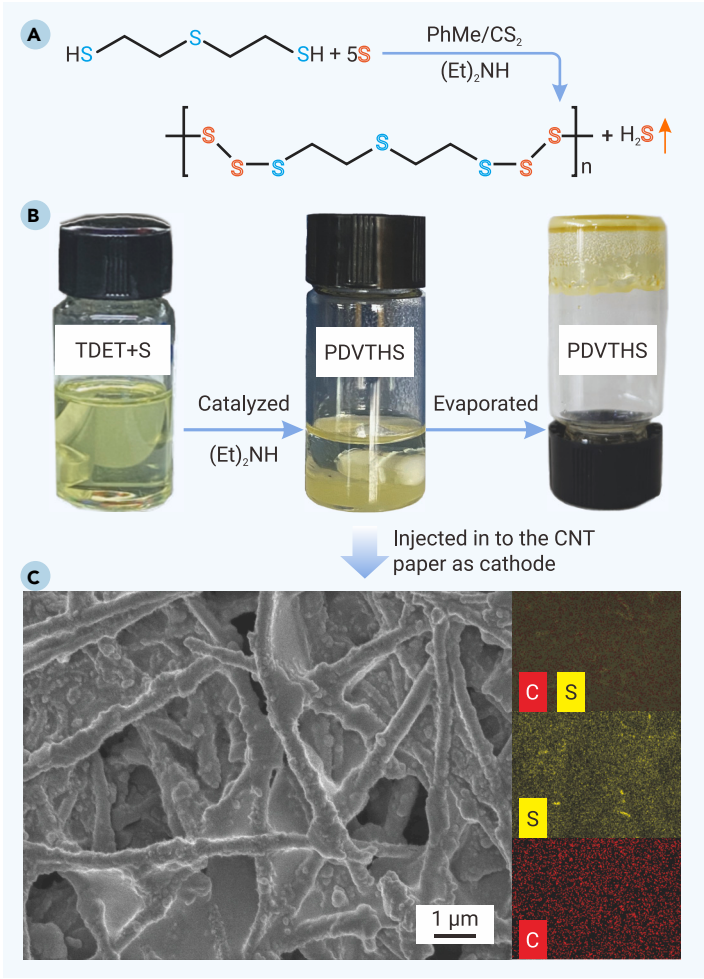

Figure 2. Conception and characteristics of the PDVTHS (A) Synthesis mechanism of polydivinylthioether hexasulfide (PDVTHS). (B) Schematic procedure with digital images. (C) SEM image of the PDVTHS-CNT cathode along with EDS elemental mapping of sulfur (yellow) and carbon (red) in the inset.

when CS_2 evaporates. Then, the target product, *PDVTHS*, is transferred to a 60° oven to dry for further detection and analysis. Figure 2B directly shows the observation of the glass vial that reactants dissolve in the solvent into a clear and transparent light yellow solution. Upon the addition of the catalyst, a distinct stratification occurs: the upper layer remains a transparent solution, while the lower layer becomes a yellow grease. After completely drying, the rubber polymer appears. SEM images reveal the micromorphology of the *PDVTHS*-CNT cathode (Figure 2C). Compared to the fresh carbon nanotubes in the carbon strips, the polymer is clearly precipitated on the CNT paper, resulting in a blurred boundary between the carbon nanotubes. Elemental analysis (EDS) reveals that S and C elements are evenly distributed on the material.

Various characterizations are conducted to certify the successful synthesis and study the chemical nature for the SCP, *PDVTHS*, based on thiol-sulfur click chemistry. As shown in Figure 3A, XRD partum reveals that *PDVTHS* has no characteristic peak of sulfur, indicating the complete consumption of sulfur and the generation of the polymer through its attachment to the S atom on the polymer chain. The broad peak at low angles of 2θ up to 20° is ascribed to scattering by the amorphous materials, revealing its polymeric nature. The broad peak of *PDVTHS*-CNT also expresses its polymeric feature. In addition, peaks from C are significantly observed at angles 2θ = 20.11°, 23°, and 26.2°. The XRD pattern of the CNT is as shown in Figure S3. To comprehensively understand the bond changes as the precursor TDET is converted to *PDVTHS*, FTIR spectroscopy is conducted (Figure 3B). It is worth noting that the peak of precursor TDET at 2,546 cm^{-1} originating from the S-H stretching vibration disappears in the *PDVTHS* spectrum. In addition, a new peak signified by S-S vibration bands appears at 833.5 cm^{-1}, implying the conversion of TDET into *PDVTHS*. In addition, the C-S bond vibration of 713.5 cm^{-1} and the C-H bond vibration of 1,415.5 cm^{-1} in *PDVTHS* are weakened compared with those in TDET, which may be attributed to the change of the degrees of freedom from TDET to *PDVTHS*.[18] We use TOF-SIMS to investigate the molecular weight and molecular formula of *PDVTHS*. As shown in Figure 3C, a molecular ion peak[7] (280 u) and excimer ion peaks (281 and 282 u) are obtained, and the molecular formula of *PDVTHS* is identified as $C_4H_8S_7$. XPS analysis (Figure 3D) shows that the signals at 284.9 and 282.8 eV belong to C-S and C-C bonds in the C 1*s* spectra of *PDVTHS*, respectively.[19,20] In S 2*p* fine spectrum analysis, 163.7 eV is a typical S 2*p* peak from the S-S bond, and a single peak with an energy separation of 1.7 eV at 162 eV confirms the presence of S-C bonds.[8,21] From TGA and DSC tests as illustrated in Figure 3E, the thermal decomposition temperature of *PDVTHS* is 268°C, which has good thermal stability. To obtain the exact element content, element analysis is conducted (Table S1). The contents of C, H, and S in *PDVTHS* are 16.773%, 2.449%, and 80.069%, respectively, which are consistent with the results of TOF-SIMS and TGA. The above characterization results indicate that the SCP *PDVTHS* has been successfully synthesized using the thiol-sulfur click chemistry method proposed here.

In this section, the electrochemical behavior of PDTVHS as a positive active material in lithium-organosulfide batteries is explored. As shown in Figure 4A, the CV curve renders two reduction peaks, labeled as ① and ② at 2.23 and 2.0 V, corresponding to the two discharging platforms of the GCD profile (Figure 4B). Platform ① represents the breaking of the S-S bond in *PDVTHS*, due to its lower bond energy, followed by the incorporation $2Li^+$ to form $LiS_2C_4H_8S_3Li$. Platform ② represents the further conversion of the intermediate products into the final discharged products (such as 2, 2′-thiobis(lithium ethiothiol) [$LiSC_4H_8S_2Li$] and Li_2S). In platform ③, the discharging products are converted back to reactant *PDVTHS*. The overall redox reaction is depicted in the inset of Figure 4B. The morphological transformation evolutions during the discharge and charge processes are investigated by a SEM. Figures 4C–4F show the morphologies of four different phases: (1) CNT paper (Figure 4C), exhibiting a typical morphology of carbon nanotubes; (2) a fresh PDVTH-CNT cathode with a uniform deposition of SCP within the CNT network (Figure 4D); (3) a cathode discharged to 1.6 V at 0.05 C (Figure 4E), where the surface morphology of the *PDVTHS*-CNT cathode returns to that of fresh CNT paper, indicating the reduction of SCP to low-order lithium polysulfides and inorganic small-molecule lithium sulfide (Li_2S_2, Li_2S); and (4) the cathode is recharged to 3 V (Figure 4F), the cross-linked polymer reappears, and the morphology is consistent with that of the pristine *PDVTHS*-CNT cathode. S 2*p* XPS contributes to identify the charged/discharged products of *PDVTHS*. For the discharged cathode, as elaborated in Figure 4G, the S $2p_{3/2}$ peak (160 eV) and S $2p_{1/2}$ peak (162 eV) are derived from Li_2S and $LiSC_4H_8S_2Li$, which are the primary discharging products. The S $2p_{3/2}$ peak (163.3 eV) can be ascribed to partially reduced lithium polysulfides (Li_2S_x, $2 \leq x \leq 4$) because of incomplete discharging, and the S $2p_{1/2}$ peak (166.9 eV) is reconfirmed in the presence of thiosulfate. The S 2*p* spectrum of the organic cathode recharged to 3 V indicates the presence of S=O around 166.2 eV stemming from the thiosulfate of the residual side reaction product. Two sets of peaks, 162.5 and 163.7 and 168.2 and 169.4 eV, both in discharged/charged cathodes, stand for the S-S and S-C bonds.[22,23]

To verify that the reaction pathway occurred according to the prediction, an *operando* Raman spectroscopy analysis was performed on the cathode of different discharging/charging depths under a CV test at 50 $\mu V\ s^{-1}$ (Figure 4H). Raman signals of 147, 217, and 353 cm^{-1} (the voltage is higher than 2.45 V) correspond to the S-C and S-S bonds of the preliminary lithiation intermediate. When discharge below 2.23 V, peaks of Li_2S (495 cm^{-1}) and low-order lithium polysulfide (Li-S-CH_2-S-CH_2-S-Li, 1, 353 cm^{-1}) appear but then disappear when the voltage recharges above 2.45 V, which can be monitored by an *operando* Raman spectral signal collection process.[24,25] During battery charging, a peak at 473 cm^{-1} is detected as the voltage rises to 2.45 V, synchronous with the relative intensity becoming stronger until the voltage rises to 3 V. This signal is assigned to the reconstituted *PDVTHS*, which disappears again after the reduction potential declines to 2.23 V, suggesting a typical reversible conversion from *PDVTHS* to the final discharged products. It is worth noting that the signal at 1,587 cm^{-1} existed in whole potential is ascribed to the ethyl thioether (-CH_2-S-CH_2-) group of intermediates, according to the Raman spectrum of the raw *PDVTHS* matrix (Figure S4). UV-vis absorption spectroscopy is utilized to validate the reaction pathway. The cathodes that are discharged to

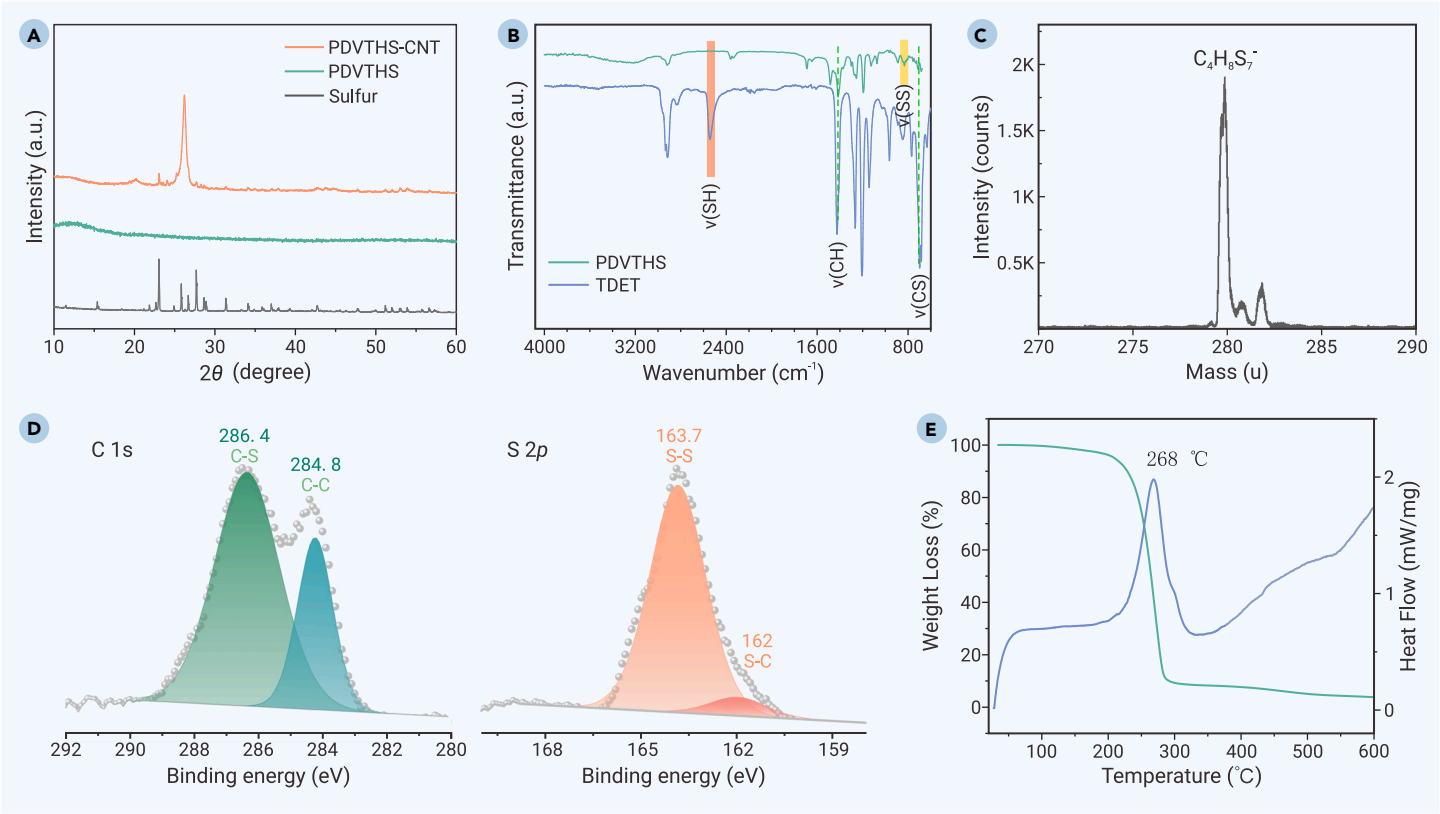

Figure 3. Characterizations of PDVTHS (A) XRD, (B) FTIR, (C) TOF-SIMS, (D) C 1s and S 2p XPS spectra, and (E) TGA curves and corresponding DSC spectrum tested in N2 with a heating rate of 10°C min^{-1}.

1.6 V after 10 cycles (noted as 10 th-DC-2.2 V in the current format) and 10 th-RC-3.0 V are selected for testing. Then, the positive plates are taken out and soaked in DOL/DME solvent. As expected, according to the color of the solution, all the electrolytes of the impregnated cathode plates are colorless and transparent (Figure S5), indicating that there is no formation of a long-chain polysulfide during the reaction or that the generated amount is very small and difficult to observe. The solution is used for UV-vis absorbable spectroscopy to further verify the products at completely discharging/recharging potentials (Figure S6).[26,27] For the cathode discharged to 1.6 V, no noticeable change is detected except the appearance of an intensity peak at 218 nm stemming from the ethyl thioether group in Li-S-CH_2-S-CH_2-S-Li. In contrast, the absorption peak of the ethyl thioether group in the cathode (positive potential at 3 V) shifts to a higher wavenumber, 227 nm, due to the different chemical environment of the *PDVTHS* molecule. Since the signal of preliminary lithiated *PDVTHS* is observed at 419 nm, experience a facile Li-chelation that polysulfide bridging Li^+ to form Li-S_3-CH_2-S-CH_2-S_3-Li owing to interference of the electrolyte, and a few lithium products (Li-S_2-CH_2-S-CH_2-S_2-Li) that have not been completely oxidized appeared at 334 nm. The results clearly indicate different electrochemical behaviors and intermediate products of *PDVTHS*. The long-chain polysulfide is absent during the battery operation process; meanwhile, in the *PDVTHS* cathode, it mainly exists in the form of a preliminary lithiation product (e.g., Li-S_2-CH_2-S-CH_2-S_2-Li) at the small peak ① and final discharging products, low-order lithium polysulfide (Li-S-CH_2-S-CH_2-S-Li) and Li_2S, at the big peak ② in the CV curve, implying that the *PDVTHS* composite architecture could effectively avoid the severe shuttling effect of long-chain polysulfides and therefore realize excellent cycling stability.

The performance of the *PDVTHS*-CNT cathode is evaluated in a lithium-organosulfide battery. Figure 5A expresses the rate capacity at various current densities ranging from 0.05 to 5 C. At lower current rates of 0.05, 0.1, 0.2, 0.5, 1, and 2 C, the cathode demonstrates excellent rate performance, with capacities of 790.5 (82.6% of theoretical capacity), 671, 649, 609, 337.5, and 200 mAh g^{-1}, respectively (Figure 5B). At higher current rates of 5 C, it has a capacity of 100 mAh g^{-1} (10.4% of theoretical capacity), which is likely due to the large electrolyte consumption. After switching back to 0.2 and 0.1 C, capacity can still recover stably to 656 and 647 mAh g^{-1}, implying that the *PDVTHS*-CNT cathode has good rate performance. The cycle properties of cathodes with different SCP area loadings (1.24, 2.48, and 3.72 mg cm^{-2}) are shown in Figure 5C. The initial capacities are 589, 530, and 457 mAh g^{-1} at 0.1 C, respectively, indicating that batteries with low active materials loaded maintain a higher capacity retention and a long cycle life. The obtained result can also be caused by a larger liquid-sulfur ratio (E/S) and lower consumption of the electrolyte. Furthermore, the properties of PDVTHS in this work are compared with those of organic materials reported in recent years based on the rate capacity (Figure 5D), and one can obviously see the excellent performance of this work. The detailed rate capacity and molecular structure have been given in Table S2. The long-term cycle performance at 0.2 C for the *PDVTHS* cathode with a 2.48 mg cm^{-2} loading is presented in Figure 5E. The initial capacity is 335 mAh g^{-1}, and after 1,000 cycles, the capacity remains at 124 mAh g^{-1}, with a capacity decay rate of only 0.063%. GCD profiles of 290–300 and 900–910 cycles are shown in the insets of Figure 5E, indicating that the battery runs steadily. The corresponding GCD profiles of difference cycles are shown in Figure S7. The corresponding specific capacities based on sulfur are characterized in Figures S8–S10. Furthermore, Figure S11 presents the EIS data for the pristine and cycled cathode, indicating that the cathode maintains good conductivity even after long-term cycling. The impedance values are listed in Table S3. These results reveal that the *PDVTHS*-CNT cathode exhibits excellent interface compatibility with the electrolyte, significantly reducing charge transfer impedance and ensuring stable reaction kinetics over long-term cycles.

CONCLUSION

In this work, we have summarized the type of alkali-catalyzed polymerization of thiol and S_8 and named it thiol-sulfur click chemistry. Under alkaline catalysis, thiol groups form highly nucleophilic sulfur anions, which then attack the less resistant S atom of the S_8 ring, resulting in polymerization. Aside from it being fast and reliable, an additional figure of merit of thiol-sulfur click chemistry is that its products exhibit decent performance of stored energy. *PDVTHS*, a

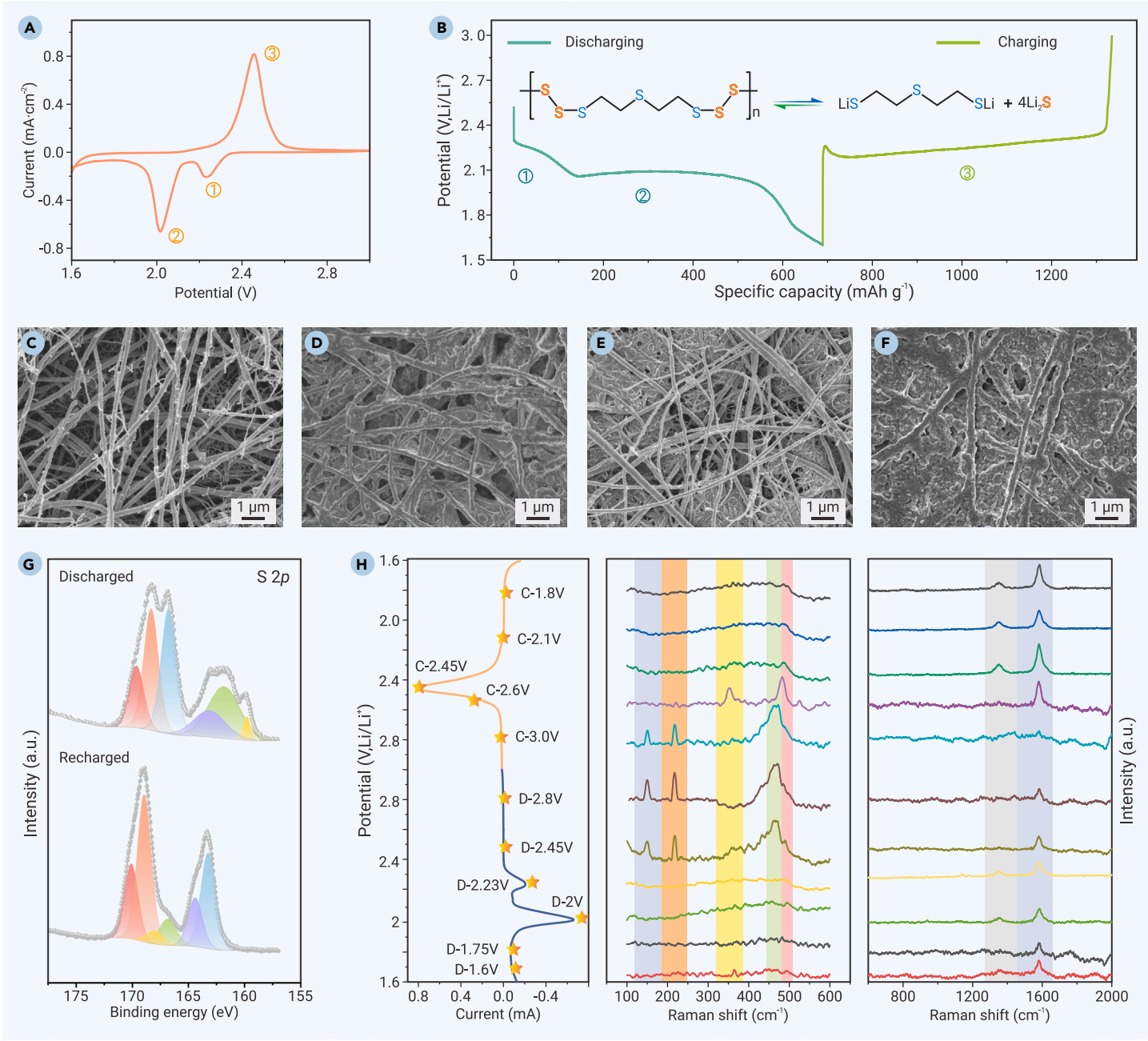

Figure 4. The study of electrochemical behavior of the PDVTHS-CNT cathode in a Li-S battery (A) CV curves performed at 50 μV s^{-1}. (B) Voltage profile cycled at 0.05 C rate with labels for the different voltages corresponding to the potentials shown in CV curves. (C) The morphology of CNT paper. (D–F) SEM images for various phases of PDVTHS-CNT cathode are shown: (D) pristine, (E) discharged to 1.6 V, and (F) recharged to 3 V. (G) S 2p XPS spectra of the completely discharged/recharged cathode after 2 cycles at 0.05 C rate. (H) *Operando* Raman spectroscopy analysis of different potentials based on CV test at 50 μV s^{-1}.

novel SCP, has been successfully synthesized using this approach. It demonstrates a high theoretical specific capacity of 957.3 mAh g^{-1}, an initial capacity of 790.5 mAh g^{-1} (82.6% of theoretical capacity), and a long-term cycling life of 1,000 cycles with a low-capacity decay rate of 0.063%. In consequence, the proposal of the new reaction pathway provides insights for the development and synthesis of other SCPs.

REFERENCES

1. Wang, Z., Fan, Q., Guo, W., et al. (2022). Biredox-Ionic Anthraquinone-Coupled Ethylviologen Composite Enables Reversible Multielectron Redox Chemistry for Li-Organic Batteries. Adv. Sci. **9**(1): 2103632. https://doi.org/10.1002/advs.202103632.
2. Zhang, K., Li, X., Yang, Y., et al. (2022). High Loading Sulfur Cathodes by Reactive-Type Polymer Tubes for High-Performance Lithiu-Sulfur Batteries. Adv. Funct. Mater. **33**(11): 2212759. https://doi.org/10.1002/adfm.202212759.
3. Tang, M., Zhu, S., Liu, Z., et al. (2018). Tailoring π-Conjugated Systems: From π-π Stacking to High-Rate-Performance Organic Cathodes. Chem **4**(11): 2600–2614.
4. Lv, X., Yang, Q., Zhang, X., et al. (2022). Acceleration of Cathode Interfacial Kinetics by Liquid Organosulfides in Lithium Metal Batteries. Angew. Chem. Int. Ed. **61**(49): e202213160. https://doi.org/10.1002/anie.202213160.
5. Otteny, F., Perner, V., Wassy, D., et al. (2019). Poly(vinylphenoxazine) as Fast-Charging Cathode Material for Organic Batteries. ACS Sustain. Chem. Eng. **8**(1): 238–247.
6. Liu, Y., Niu, Z., Dai, G., et al. (2021). Phenothiazine-based copolymer with redox functional backbones for organic battery cathode materials. Mater. Today Energy **21**: 100812. https://doi.org/10.1016/j.mtener.2021.100812.
7. Ren, Y., Si, Y., Guo, W., et al. (2023). A cyclic organosulfide cathode with ultrastable cycling performance in lithium batteries. Chem. Commun. **59**(22): 3289–3292.
8. Zou, R., Liu, W., and Ran, F. (2023). Selenium-doped cathode materials with polyaniline skeleton for lithium-organosulfur batteries. J. Energy Chem. **79**(4): 148–157.
9. Zou, R., Zhang, J., Zheng, Y., et al. (2024). Tailoring Interfacial Electric Field by Gold Nanoparticles Enable Electrocatalytic Lithium Polysulfides Conversion for Lithium-Sulfur Batteries. Small **20**(29): 2312102. https://doi.org/10.1002/smll.202312102.

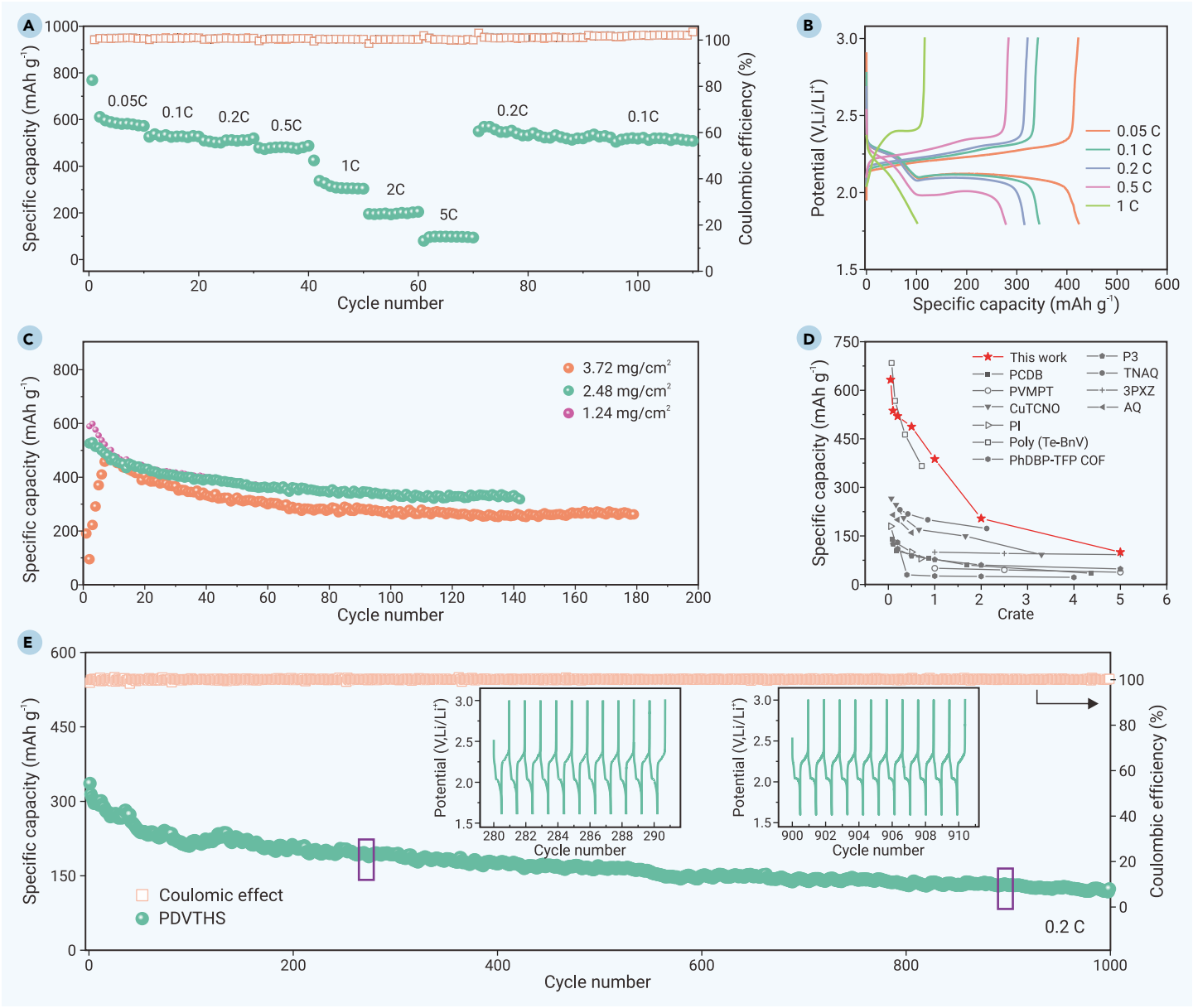

Figure 5. Electrochemical behavior evaluation (A and B) Rate capacity (A) and corresponding GCD profiles (B). (C) Cycling performance under different mass loadings at 1 C (1 C = 975.3 mA g^{-1}) within a voltage window of 1.6–3.0 V. (D) Comparison of rate performance of the robust PDVTHS electrodes in this work and other organic cathodes recently reported. (E) Long-term cycling performance.

10. Xu, Z.Q., Zou, R., Liu, W.W., et al. (2023). Design of atomic cobalt selenide-doped sulfurized polyacrylonitrile cathode with enhanced electrochemical kinetics for high performance lithium-SPAN batteries. Chem. Eng. J. ***471***: 144581. https://doi.org/10.1016/j.cej.2023.144581.
11. Devaraj, N.K., and Finn, M.G. (2021). Introduction: Click Chemistry. Chem. Rev. ***121***(12): 6697–6698.
12. Uchiyama, M., Osumi, M., Satoh, K., et al. (2020). Thiol-Ene Cationic and Radical Reactions: Cyclization, Step-Growth, and Concurrent Polymerizations for Thioacetal and Thioether Units. Angew. Chem. Int. Ed. ***59***(17): 6832–6838.
13. Mather, B.D., Viswanathan, K., Miller, K.M., et al. (2006). Michael addition reactions in macromolecular design for emerging technologies. Prog. Polym. Sci. ***31***(5): 487–531.
14. Zhao, L., Li, Y., Yu, M.M., et al. (2023). Electrolyte-Wettability Issues and Challenges of Electrode Materials in Electrochemical Energy Storage, Energy Conversion, and Beyond. Adv. Sci. ***10***(17): e2300283.
15. Yeo, H., and Khan, A. (2020). Photoinduced Proton-Transfer Polymerization: A Practical Synthetic Tool for Soft Lithography Applications. J. Am. Chem. Soc. ***142***(7): 3479–3488.
16. Hoogenboom, R. (2023). Click chemistry in polymer science. Chem ***9***(9): 2416–2424.
17. Chung, W.J., Griebel, J.J., TaeKim, E., et al. (2013). The use of elemental sulfur as an alternative feedstock for polymeric materials. Nat. Chem. ***5***(6): 518–524.
18. Bhargav, A., Chang, C.H., Fu, Y., et al. (2019). Rationally Designed High-Sulfur-Content Polymeric Cathode Material for Lithium-Sulfur Batteries. ACS Appl. Mater. Inter. ***11***(6): 6136–6142.
19. Khanam, Z., Xiong, T., Yang, F., et al. (2024). Endogenous Interfacial Mo-C/N-Mo-S Bonding Regulates the Active Mo Sites for Maximized Li^+ Storage Areal Capacity. Small ***20***(31): 202311773. https://doi.org/10.1002/smll.202311773.
20. Yang, H., Xiong, T., Zhu, Z., et al. (2022). Deciphering the lithium storage chemistry in flexible carbon fiber-based self-supportive electrodes. Carbon Energy ***4***(5): 820–832.
21. Chen, L., He, T., Liao, K., et al. (2024). A Ternary (P, Se, S) Covalent Inorganic Framework as a Shuttle Effect-Free Cathode for Li-S Batteries. Adv. Mater. ***36***(4): e2308587. https://doi.org/10.1002/adma.202308587.
22. Hu, H., Zhao, B., Cheng, H., et al. (2019). A robust 2D organic polysulfane nanosheet with grafted polycyclic sulfur for highly reversible and durable lithium-organosulfur batteries. Nano Energy ***57***: 635–643.
23. Chen, P., Wu, Z., Guo, T., et al. (2021). Strong Chemical Interaction between Lithium Polysulfides and Flame-Retardant Polyphosphazene for Lithium-Sulfur Batteries with Enhanced Safety and Electrochemical Performance. Adv. Mater. ***33***(9): 2007549. https://doi.org/10.1002/adma.202007549.
24. Wang, T., Zhang, Q., Zhong, J., et al. (2021). 3D Holey Graphene/Polyacrylonitrile Sulfur Composite Architecture for High Loading Lithium Sulfur Batteries. Adv. Energy Mater. ***11***(16): 2100448. https://doi.org/10.1002/aenm.202100448.
25. Haldar, S., Bhauriyal, P., Ramuglia, A.R., et al. (2023). Sulfide-Bridged Covalent Quinoxaline Frameworks for Lithium-Organosulfide Batteries. Adv. Mater. ***35***(16): 2210151. https://doi.org/10.1002/adma.202210151.

26. Zhou, J., Qian, T., Xu, N., et al. (2017). Selenium-Doped Cathodes for Lithium-Organosulfur Batteries with Greatly Improved Volumetric Capacity and Coulombic Efficiency. Adv. Mater. ***29***(33): 1701294. https://doi.org/10.1002/adma.201701294.
27. Long, B., Ma, J., Song, T., et al. (2021). Bifunctional polyvinylpyrrolidone generates sulfur-rich copolymer and acts as "residence" of polysulfide for advanced lithium-sulfur battery. Chem. Eng. J. ***414***: 128799. https://doi.org/10.1016/j.cej.2021.128799.

ACKNOWLEDGMENTS

This work was partly supported by the National Natural Science Foundation of China (52463013 and 52073133), the Major Science and Technology Project of Gansu Province (22ZD6GA008), the Incubation Program of Excellent Doctoral Dissertation-Lanzhou University of Technology. The funders had no role in study design, data collection and analysis, decision to publish, or preparation of the manuscript.

AUTHOR CONTRIBUTIONS

R.Z.: Writing-orginial draft, Methodology, Investigation, Formal analysis, Data curation, and Conceptualization. W.W.L.: Software and Resources. F.R.: Writing-review & editing, Supervision, Project administration, Funding acquisition, and Conceptualization.

DECLARATION OF INTERESTS

The authors declare no conflicts of interest.

SUPPLEMENTAL INFORMATION

It can be found online at https://doi.org/10.1016/j.xinn.2024.100765.